

Mass loss in main-sequence B stars

Jiří Krtička

Ústav teoretické fyziky a astrofyziky, Masarykova univerzita, CZ-611 37 Brno, Czech Republic, e-mail: krticka@physics.muni.cz

Received

ABSTRACT

We calculate radiatively driven wind models of main-sequence B stars and provide the wind mass-loss rates and terminal velocities. The main-sequence mass-loss rate strongly depends on the stellar effective temperature. For the hottest B stars the mass-loss rate amounts to $10^{-9} M_{\odot} \text{ year}^{-1}$, while for the cooler ones the mass-loss rate is by more than three orders of magnitude lower. Main sequence B stars with solar abundance and effective temperatures lower than about 15 000 K (later than the spectral type B5) do not have any homogeneous line-driven wind. We predict the wind mass-loss rates for the solar chemical composition and for modified abundance of heavier elements to study the winds of chemically peculiar stars. The mass-loss rate may both increase or decrease with increasing abundance depending on the importance of the induced emergent flux redistribution. Stars with overabundant silicon may have homogeneous winds even below the solar abundance wind limit at 15 000 K. The winds of main-sequence B stars lie below the static limit, i.e., a static atmosphere solution is also possible. This points to an important problem of initiation of these winds. We discuss the implications of our models for the rotational braking, filling the magnetosphere of Bp stars and for chemically peculiar stars.

Key words. stars: winds, outflows – stars: mass-loss – stars: early-type – hydrodynamics

1. Introduction

Line driven winds are mainly studied in the most luminous hot stars. These stars have strong winds which are easily attainable to observations and which significantly influence the stellar evolution. However, also winds of less luminous stars, especially main-sequence B stars, have considerable observational and theoretical consequences. Although the winds in these stars do not manifest themselves by prominent spectral features or do not have decisive influence on the way how the stars evolve, weaker winds affect a number of observational phenomena that gain considerable astrophysical attention.

Main sequence B stars lie at the boundary between luminous O stars where the radiative force expels huge amount of mass out from the star (Puls et al. 2008) and main-sequence A stars, where the minute effect of the radiative levitation horizontally redistributes the elements in remarkable surface spots (Michaud 2004). It has long been speculated that the outflow is a missing ingredient that is needed for a quantitative explanation of resulting abundance anomalies. Such explanation faces a strong problem in missing consistent theoretical predictions of wind mass-loss rates at low luminosity.

Traditionally, two parameters are invoked to explain all aspects of the evolution of single stars: the initial mass and chemical composition. However, now it seems that at least a third parameter is essential for the explanation of the single star evolution: the initial stellar angular momentum (Meynet et al. 2006). Consequently, rotation becomes one of the crucial parameters of evolutionary models. The stellar rotation may not only contribute to the internal mixing of chemical elements, but it may also bring a star to the proximity of the critical rotation (Ekström et al. 2012). Fast rotation is also a prerequisite for the collapsar model of gamma-ray bursts (Yoon et al. 2006). Unfortunately, the evolutionary time scale is hopelessly long to

test the predictions of rotational velocity evolution models directly. However, there is one exception: the rotationally modulated light variations of chemically peculiar stars provide us a powerful clock, that is able to reveal even the minute change of the rotational period. Studies based on such a clock (Pyper et al. 1998, Mikulášek et al. 2011) have shown period variations that might be connected with angular momentum loss via magnetized stellar wind. However, precise mass-loss rate predictions for these stars are missing to test the angular momentum loss hypothesis quantitatively.

As a result of its low density, the wind material could be trapped in the magnetospheres of Bp stars. Resulting magnetospheric clouds are the prime origin of the light variability of σ Ori E (Landstreet & Borra 1978, Townsend et al. 2005). Detailed properties of these clouds, such as the timescale of their build-up, are poorly constrained due to uncertain mass-loss rates at low luminosity.

Last but not least, winds of low luminous hot stars are also appealing theoretically. They provide a unique environment, where many astrophysical phenomena can be manifested, including the particle collisions leading to the multicomponent nature of the flow (e.g., Springmann & Pauldrach 1992, Krtička et al. 2006), or the line Doppler heating influencing the wind temperature (Gayley & Owocki 1994). Note however, that because the latter two effects occur in the outer wind, they typically do not affect the mass-loss rate.

Stellar winds of main-sequence B stars are difficult to study observationally. The $H\alpha$ line, which is a crucial mass-loss rate indicator in O stars, is not usable for the mass-loss rate of the order of $10^{-8} M_{\odot} \text{ year}^{-1}$ or lower (Puls et al. 2008), i.e., in the domain of main-sequence B stars. Moreover, the mass-loss rate determination of main-sequence B stars from observations may be uncertain not only as the result of the effect of clumping on the line-profiles (Sundqvist et al. 2011, Šurlan et al. 2012), but also

as the result of the weak wind problem (e.g., Bouret et al. 2003, Martins et al. 2005, Marcolino et al. 2009). The latter problem is connected with observed ultraviolet wind line profiles in low-luminosity O stars, which are too weak compared with theory. The weak mass-loss rates inferred from weak ultraviolet lines are (at least in one case) supported by the mass-loss rate derived from Br γ line (Najarro et al. 2011).

On the other hand, there are independent observational indications (Huenemoerder et al. 2012, Gvaramadze et al. 2012) showing that the ultraviolet line profiles significantly underestimate the mass-loss rate in low-luminosity O stars. The weakness of the ultraviolet line profiles can be then explained by the high wind temperature, as a result of the shock heating in the medium with such a low density, that is not able to cool down radiatively (Lucy & White 1980, Cohen et al. 2008, Krtićka & Kubát 2009b, Lucy 2012). From this point of view the theoretical models provide the reliable choice for the estimation of B star mass-loss rates.

To improve the situation with poorly known wind parameters in main-sequence B stars, we provide here mass-loss rate estimates based on our own NLTE wind code.

2. Description of models

For the prediction of main-sequence B star mass-loss rates we apply NLTE wind models of Krtićka & Kubát (2010) with a comoving frame (CMF) line force. Our wind models assume stationary, and spherically symmetric flow. They enable us to selfconsistently predict wind structure and wind parameters just from the basic stellar parameters, i.e., the effective temperature, mass, radius, and chemical composition.

The ionization and excitation state of considered elements is derived from the statistical equilibrium (NLTE) equations. For this purpose we adopted a set of ionic models from the TLUSTY grid of model stellar atmospheres (Lanz & Hubeny 2003, 2007), which was extended using the data from the Opacity and Iron Projects (Seaton et al. 1992, Hummer et al. 1993). For phosphorus we employed data described by Pauldrach et al. (2001).

The NLTE model atmosphere emergent fluxes, which serve as a lower boundary condition of the radiative transfer equation in the wind, are calculated by the TLUSTY code (Lanz & Hubeny 2007) for the same stellar parameters (the effective temperature, surface gravity and chemical composition) as the wind models.

The line radiative force is calculated using the solution of the spherically symmetric CMF radiative transfer equation (Mihalas et al. 1975). The corresponding line data were extracted from the VALD database (Piskunov et al. 1995, Kupka et al. 1999). We apply the electron thermal balance method (Kubát et al. 1999) for the calculation of the radiative cooling and heating. These terms are calculated with the occupation numbers derived from the statistical equilibrium equations.

The continuity equation, equation of motion, and energy equation are solved iteratively using the Newton-Raphson method. An accelerating outflow is assumed in the first step of iterations. As a result of iterations we obtain the wind density, velocity, and temperature structure that satisfy the hydrodynamical equations. We have not found any case when the derived solution (faster than the radiative-acoustic waves at outer edge, Abbott 1980) would not be unique, i.e., the final converged solution does not depend on a particular choice of initial conditions. We assume homogeneous flow, i.e., we neglect possible differences in velocities of individual components. This is legitimate here, as we are interested mainly in the mass-loss rates.

Table 1. Stellar parameters of the model grid

Model	Sp. Type	T_{eff} [K]	M [M_{\odot}]	R_* [R_{\odot}]	$\log(L/L_{\odot})$	v_{esc} [km s^{-1}]
T30	B0	30 000	14.73	5.84	4.39	960
T28		28 000	12.69	5.34	4.20	940
T26	B1	26 000	10.88	4.87	3.99	910
T24		24 000	9.26	4.45	3.77	880
T22		22 000	7.84	4.07	3.54	850
T20		20 000	6.60	3.71	3.30	820
T18		18 000	5.52	3.39	3.03	790
T16	B5	16 000	4.58	3.09	2.75	750
T14	B6	14 000	3.76	2.80	2.43	720

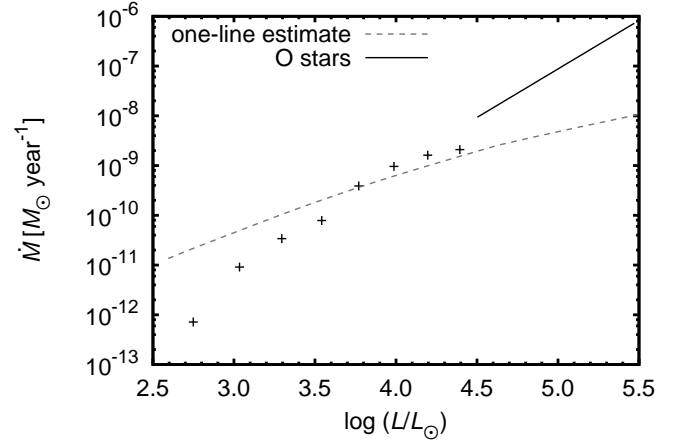


Fig. 1. Predicted mass-loss rates for solar metallicity as a function of the stellar luminosity. Overplotted (solid line) is the fit to main-sequence O star mass-loss rates (Krtićka & Kubát 2012). The dashed line denotes the one-line mass-loss rate estimate (Krtićka & Kubát 2009a).

The stellar parameters of the considered model grid are given in Table 1. Here we also provide the corresponding spectral types for selected models. The effective temperature T_{eff} covers the range of earlier B stars, and the stellar mass M and radius R_* were calculated from the interpolation formulas derived for main-sequence stars by Harmanec (1988) with the effective temperature as a parameter. For the calculation of both wind and atmosphere models we assume a solar chemical composition after Asplund et al. (2009). We also calculated additional models with modified abundance of the elements that are most important for the line driving, i.e., carbon, nitrogen, oxygen, silicon, sulfur, and iron. The range of considered abundances of these elements was partially motivated by that found typically on the surface of chemically peculiar stars (e.g., Briquet et al. 2004, Lehmann et al. 2007, Bohlender et al. 2010).

3. Mass-loss rates

The predicted mass-loss rates \dot{M} for B stars with solar metallicity in Table 2 nicely follow the O star mass-loss rate – luminosity relationship (Fig. 1). The mass-loss rates of solar metallicity B stars can be fitted via the formula

$$\log\left(\frac{\dot{M}}{1 M_{\odot} \text{ year}^{-1}}\right) = a + b\left(\frac{T_{\text{eff}}}{10^4 \text{ K}}\right) + c\left(\frac{T_{\text{eff}}}{10^4 \text{ K}}\right)^2, \quad (1)$$

Table 2. Predicted mass-loss rates and terminal velocities for different abundances and different effective temperatures. Mass-loss rates are given in the units of $10^{-11} M_{\odot} \text{ year}^{-1}$. The terminal velocities v_{∞} are given in the units of km s^{-1} . The terminal velocity in parentheses denotes a model in which it was not possible to calculate a monotonic solution to large radii (see the text).

Model	Solar		[C/H] = -1		[C/H] = 1		[N/H] = -1		[N/H] = 1		[O/H] = -1		[O/H] = 1	
	\dot{M}	v_{∞}	\dot{M}	v_{∞}	\dot{M}	v_{∞}	\dot{M}	v_{∞}	\dot{M}	v_{∞}	\dot{M}	v_{∞}	\dot{M}	v_{∞}
T30	210	3650	190	2280	210	5490	120	4010	370	4410	100	4110	190	4390
T28	160	4380	150	2620	110	8610	67	4540	160	5520	160	4500	130	4260
T26	96	3070	60	2400	60	(2340)	64	(2440)	90	4790	100	2990	79	3040
T24	39	1700	23	1720	42	1820	4.8	2040	38	3620	25	1850	39	1700
T22	7.9	1690	8.5	1580	14	1490	0.71	1760	14	2730	6.5	1820	12	1600
T20	3.4	1290	2.3	1250	1.5	1410	1.6	1260	6.4	1720	3.2	1300	3.6	1200
T18	0.91	820	0.42	460	0.58	900	0.51	760	1.8	1120	0.84	720	0.88	790
T16	0.072	(240)	0.023	(180)	0.06	520	0.038	(230)	0.17	420	0.058	(240)	0.06	(230)
T14	no wind		no wind		no wind		no wind		no wind		no wind		no wind	
Model	[Si/H] = 1		[Si/H] = 2		[Si/H] = 3		[S/H] = -1		[S/H] = 1		[Fe/H] = 1		[Fe/H] = 2	
	\dot{M}	v_{∞}	\dot{M}	v_{∞}	\dot{M}	v_{∞}	\dot{M}	v_{∞}	\dot{M}	v_{∞}	\dot{M}	v_{∞}	\dot{M}	v_{∞}
T30	250	4020	320	4490	490	2910	180	3720	380	3390	230	3040	1700	1720
T28	180	5510	210	5180	240	3200	130	4640	280	3850	140	3570	370	1910
T26	110	(5270)	150	3720	160	3070	83	3220	170	2820	83	3060	57	2390
T24	54	4580	81	(1620)	77	2450	29	1760	81	1710	31	1790	16	1740
T22	21	4020	23	6390	9.9	2250	5.3	1820	22	1730	6	1900	8.5	1690
T20	7.5	3630	8.4	7740	4.6	380	3	1270	4.5	1360	2.6	1320	1.8	1290
T18	3.1	1990	3.6	5270	1.9	510	0.84	790	1.4	830	0.74	830	0.39	790
T16	0.7	1400	0.7	2440	0.17	(170)	0.056	(240)	0.085	(270)	0.041	(250)	no wind	
T14	0.01	650	0.004	1290	0.002	1550	no wind		no wind		no wind		no wind	

Table 3. Line force multipliers for the models with solar metallicity

Model	k	α	\bar{Q}
T30	0.024	0.635	35
T28	0.019	0.670	54
T26	0.044	0.610	95
T24	0.38	0.435	110
T22	0.20	0.46	61
T20	0.60	0.390	95
T18	2.50	0.295	130
T16	29.5	0.140	210

where

$$a = -22.7, \quad b = 8.96, \quad c = -1.42. \quad (2)$$

The predicted mass-loss rates can be compared with the mass-loss rate estimate corresponding to one optically thick line $\dot{M} = 8\pi^2 R_*^2 \nu_{ij} H_c(\nu_{ij}) / c^2$ (Krtićka & Kubát 2009a, Eq. (11) therein). In this formula $H_c(\nu_{ij})$ is the flux at the line frequency ν_{ij} , however in Fig. 1 we use the maximum product of flux and frequency giving the maximum mass-loss rate with one optically thick line. For B stars with higher luminosities this one-line mass-loss rate estimate roughly corresponds to the predicted mass-loss rate because there are just few lines that drive the wind. For stars with lower luminosities the one-line mass-loss rate estimate overestimates the mass-loss rate because in these stars even the strongest lines become optically thin and their positions do not correspond to the maximum product $\nu H_c(\nu)$.

In main-sequence B stars the wind mass-loss rate significantly decreases with decreasing effective temperature (or luminosity). For a factor of two decrease in the effective temperature the decrease in mass-loss rates is by more than three orders of magnitude. We were not able to find any wind solution for solar metallicity model T14. This indicates that homogeneous wind is not possible for $T_{\text{eff}} \lesssim 15\,000\text{ K}$.

In Table 3 we provide the radiative force multipliers (Castor, Abbott & Klein 1975, Abbott 1982) corresponding to our solar-metallicity models. The force multipliers describe the line distribution function (Puls et al. 2000), but in our approach we simply select such force multipliers that provide the best fit of wind mass-loss rate and terminal velocity derived in models with CMF line force. The parameter α decreases with the effective temperature to account for the decrease of the wind terminal velocity. To compensate for this the line force parameter k on average increases with decreasing effective temperature. From this point of view the \bar{Q} parameter of Gayley (1995) is advantageous, because its variations are much weaker in considered stars, $\bar{Q} \approx 100$ (see Table 3, where we provide $\bar{Q} = [(1 - \alpha)k(c/v_{\text{th}})^{\alpha}]^{1/(1-\alpha)}$, where the fiducial hydrogen thermal speed is $v_{\text{th}} = \sqrt{2kT_{\text{eff}}/m_{\text{H}}}$).

There are not many mass-loss rate predictions that can be compared with Eq. (1). Vink et al. (2001) predict for the T30 model a mass-loss roughly by a factor 2 higher, but the T30 model is slightly outside the model grid considered by them. Pauldrach et al. (2001) for the model with $T_{\text{eff}} = 30\,000\text{ K}$ predict the mass-loss rate which by a factor of 4 higher than that of T30 model, but for a radius by a factor of 2 higher. After correcting for the dependence of the mass-loss rate on radius (assuming a rough dependence $\dot{M} \sim L^2$, Krtićka & Kubát 2012) this gives the mass-loss rate which is by a factor of 5 lower. Extrapolating the rates of Unglaub (2008) again outside their assumed grid our predictions are about a factor of 5 higher for the model T30, while being by about of factor 3 higher for $T_{\text{eff}} = 25\,000\text{ K}$. Finally, for $T_{\text{eff}} = 30\,000\text{ K}$ our models predict roughly one eighth of the rates predicted by de Jager et al. (1988), while for $T_{\text{eff}} = 22\,000\text{ K}$ our results are nearly the same.

In Fig. 2 we plot the relative contribution of individual elements to the radiative force in the models with solar chemical composition. The relative contribution is plotted at the critical point, where the mass-loss rate of our models is determined. The contribution of individual elements to the radiative force is a strong function of the effective temperature. Carbon and ni-

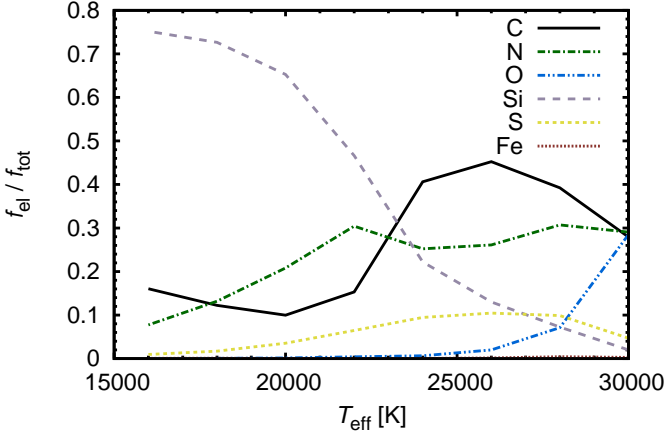


Fig. 2. The relative contribution of individual elements to the radiative force at the critical point as a function of the effective temperature. Models with solar abundance are plotted here. The contribution of iron is negligible.

nitrogen dominate the radiative force in the hottest B stars with $T_{\text{eff}} \approx 30\,000$ K, while in the stars with $T_{\text{eff}} \lesssim 22\,000$ K the lines of silicon dominate the radiative driving.

Contrary to O stars, there are only few lines that drive the wind in B stars. Iron, which dominates at higher mass-loss rates (e.g., Vink et al. 2001), has a negligible contribution to the radiative force in B stars, because (as a result of its lower abundance compared to CNO elements) most of the iron lines become optically thin. However, this is not the only reason for a low contribution of iron to the radiative force in B stars, because iron has nearly the same abundance as silicon which dominates the line driving in cooler B stars. Contrary to lighter elements like silicon or carbon, iron ions do not have allowed transitions between the most populated ground level and excited levels with the lowest energies. Consequently, the iron resonance lines have wavelengths below the Lyman limit, where the stellar radiative flux is too low at given effective temperatures and do not contribute significantly to the radiative force.

A similar situation occurs also for oxygen, where the most abundant ion in B star wind O III has the resonance lines in the Lyman continuum. On the other hand, carbon, nitrogen and silicon have strong resonance lines in the Balmer continuum, therefore they significantly contribute to the radiative force. The importance of silicon is connected with the fact that Si IV resonance lines lie close to the flux maximum. On the other hand, the importance of carbon peaks at around $T_{\text{eff}} = 25\,000$ K, where the relative contribution of resonance C IV lines at 1548 Å and 1551 Å is the strongest, while these lines become optically thin at lower effective temperatures due to the ionization shift from C IV to C III.

These results are demonstrated also in Table 4, where we list the strongest lines that drive wind in the region of the critical point. These lines can be used as a potential wind indicators in B stars. On the other hand, their absence in the spectra does not mean that the wind does not exist, because we neglected other potentially important effects, for example the wind X-ray ionization in the outer parts of the wind (e.g., Oskinova et al. 2011, see also Sect. 6.1).

The common belief is that the mass-loss rate increases with increasing metallicity due to strengthening of the line absorption. While this is true in most cases (e.g., Vink et al. 2001,

Table 4. The strongest lines in the solar-metallicity models

Model	lines (ions and wavelengths in Å)
T30	C III 977, 1176; C IV 1548, 1551; N III 990, 992; N IV 765, 923; O III 833, 834, 835; O IV 788, 790; P V 1118, 1128; S V 786
T28	C III 977, 1176; C IV 1548, 1551; N III 990, 992; Si IV 1394, 1403; P V 1118; S IV 1063, 1073
T26	C III 977, 1176; C IV 1548, 1551; N III 990, 992; Si IV 1394, 1403; S IV 1063, 1073
T24	C III 977, 1176; C IV 1548, 1551; N III 990, 992; Si IV 1128, 1394, 1403; S IV 1063, 1073
T22	C III 977; C IV 1548, 1551; N III 990, 992; Si IV 1394, 1403; S IV 1063, 1073
T20	C III 977; N III 990, 992; Si IV 1394, 1403; S IV 1073
T18	C III 977; N III 990, 992; Si IV 1394, 1403
T16	C III 977; N III 990, 992; Si III 1207; Si IV 1394, 1403

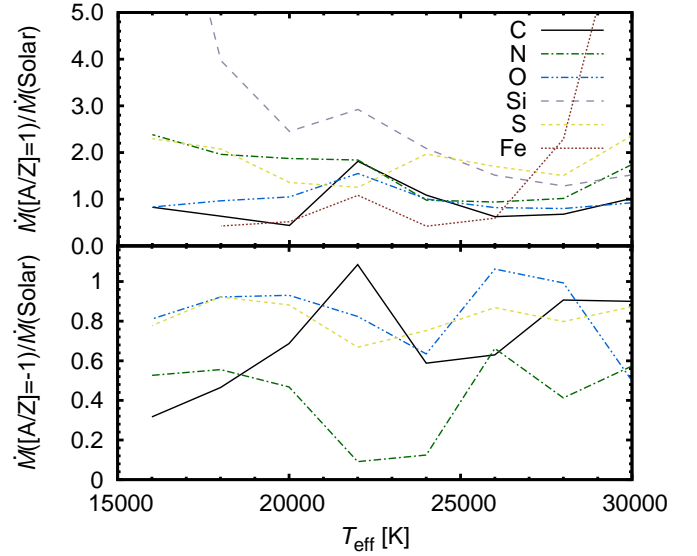


Fig. 3. The ratio of the mass-loss rate calculated with enhanced abundance of a given element by a factor of ten (*upper panel*) and with reduced abundance by a factor of ten (*lower panel*) to the mass-loss rate for a solar chemical composition as a function of stellar effective temperature.

Unglaub 2008), Fig. 3 shows that this is not always the case in the domain of main-sequence B stars. In several cases the mass-loss rate decreases with increasing abundance. This is caused by the influence of abundance on the emergent flux from the stellar atmosphere. Typically, the increase of abundance causes the flux redistribution from the far ultraviolet part of the spectrum (where most of the flux is emitted) to the near ultraviolet one and the visual one. If the redistribution is strong enough, it may affect the radiative force. We note that the same effect causes the light variability of chemically peculiar stars (e.g., Peterson 1970, Molnar 1973). Moreover, the strengthening of atmospheric lines with increasing abundance lowers the line flux and hence the radiative force if these lines significantly contribute to the radiative driving (Babel 1996).

The increase of the carbon abundance causes the atmosphere flux redistribution from the wavelengths shorter than 1100 Å to longer wavelengths causing the decrease of the radiative force. Interestingly, also the decrease of carbon abundance causes the decrease of the radiative force as a result of the decrease of

the line absorption. This effect is apparent in the models T16-T20 and T26-T30, whereas it is suppressed by a strengthening of CIV lines in the models T22 and T24 with overabundant carbon $[C/H]=1$. On the other hand, nitrogen, oxygen, and sulfur do not significantly influence the emergent atmosphere flux. Consequently, in this case indeed the radiative force increases with increasing abundance of these elements. Silicon influences the emergent atmospheric flux for higher abundances $[Si/H] \gtrsim 2$. As the result, the mass-loss rate depends on the silicon abundance strongly only when the silicon is not overabundant significantly, i.e., for $[Si/H] \lesssim 1$. Most interestingly, the mass-loss rate decreases with increasing iron abundance, even if the iron does not contribute to radiative force. This is again caused by the redistribution of the atmosphere radiative flux from the far-ultraviolet region to the near-ultraviolet and optical ones as a result of flux blocking by numerous iron lines.

The increase of abundance of heavier elements (with exception of silicon) does not help to find a wind solution for model T14. This is denoted as “no wind” in Table 2. Only stars enhanced by silicon can drive a homogeneous wind at $T_{\text{eff}} = 14\,000\text{ K}$, because silicon dominates the line force at this temperature.

The dependence of the mass-loss rate on the metallicity has significant consequences for chemically peculiar stars. The abundance of elements, most notably that of silicon and iron, vary with location on the stellar surface (e.g., Khokhlova et al. 2000, Lehmann et al. 2007). Consequently, the wind mass flux is variable over the surface. For helium-rich stars where the abundances of silicon and helium are typically anticorrelated this means, that the wind blowing from helium rich regions is weaker than that from helium poor ones. In magnetic stars also the tilting of the flow under the influence of the magnetic field (Owocki & ud-Doula 2004) influences the mass-loss rate.

We provide also the wind terminal velocities v_{∞} derived from our models (see Table 2). The terminal velocities are sensitive to the ionization structure of the outer wind, possibly leading to the scatter of the observed $v_{\infty}/v_{\text{esc}}$ ratio in O stars (Lamers et al. 1995). This effect may explain some variations of v_{∞} seen in Table 2. Since in our case the winds are driven mostly by optically thick lines, the corresponding value of the effective line force parameter $\alpha \rightarrow 1$ indicates from simple scaling $v_{\infty} \sim \alpha/(1-\alpha)Z$ (Puls et al. 2000) even stronger sensitivity of v_{∞} on abundance. However, in many cases the wind may not reach this terminal velocity either as a result of an inefficient X-ray cooling or due to multicomponent effects (see Sect. 6.1). This is also the reason why we argue that the discussion of terminal velocities that are lower than the escape speed v_{esc} in some cases (see Table 1) would be very preliminary.

In some cases the radiative force in the outer wind parts is not strong enough to maintain an accelerated wind flow. In such case a kink in the velocity profile occurs (Feldmeier & Shlosman 2000) and wind velocity decreases in the outer parts of the wind (see Fig. 4). For these models the terminal velocity in Table 2 corresponds to the maximum wind velocity and is given in parentheses. This typically occurs in the wind models T16. In the case of T16 models the wind velocity is lower than the escape one v_{esc} (see Table 1) and the wind may never leave the star. We note that our CMF procedure allows to calculate the radiative force in accelerating wind only, consequently the models in Fig. 4 were derived assuming Sobolev line force with CMF correction.

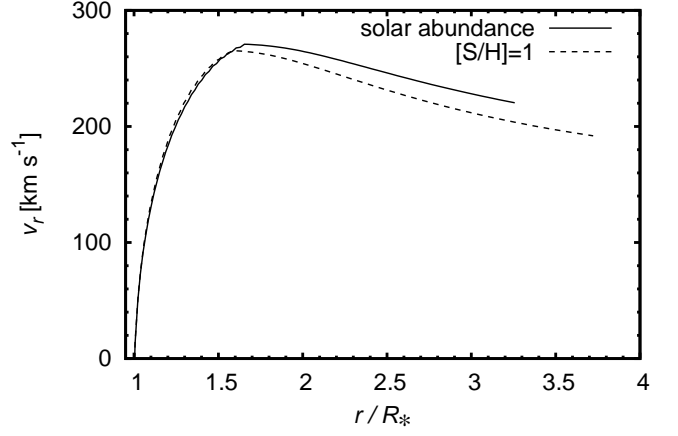


Fig. 4. The dependence of the radial wind velocity on radius in selected T16 wind models with kink for model with solar chemical composition (solid line) and with $[S/H]=1$ (dashed line).

4. The wind limit at $T_{\text{eff}} \approx 15\,000\text{ K}$

We were not able to find a wind solution for stars with $T_{\text{eff}} < 16\,000\text{ K}$ (except for the silicon rich ones). This indicates, that these stars do not have any wind. Therefore, that is why we provide additional tests for these stars, and compare the radiative force with the gravity. The winds are only possible when the magnitude of the radiative acceleration g^{rad} is greater than the magnitude of the gravity acceleration g ,

$$g^{\text{rad}} > g. \quad (3)$$

To enable the calculation of the radiative force even in the case when the wind does not exist, the hydrodynamical variables (velocity, density, and the temperature) are kept fixed during the tests. The velocity structure of our test models is given by an artificial velocity law

$$v(r) = 10^{-3} \sqrt{\frac{5}{3} \frac{kT_{\text{eff}}}{m_H}} + 2 \times 10^8 \text{ cm s}^{-1} \frac{r - R_*}{R_*}, \quad (4)$$

where T_{eff} is the stellar effective temperature, R_* the stellar radius, and m_H the mass of the hydrogen atom. The selection of such specific velocity law does not significantly influence our results. The density structure is obtained from the equation of continuity. In these test models we assume a constant wind temperature $\frac{2}{3}T_{\text{eff}}$, and the electron density is consistently calculated from the ionization balance. Since for these wind tests we do not solve the equation of motion, it is necessary to specify wind mass-loss rate for which the wind existence is tested. For each set of stellar parameters these mass-loss rates are $10^{-12} M_{\odot} \text{ year}^{-1}$, $10^{-13} M_{\odot} \text{ year}^{-1}$, $10^{-14} M_{\odot} \text{ year}^{-1}$, and $10^{-15} M_{\odot} \text{ year}^{-1}$.

The wind tests support our expectations from the previous section. The wind is possible for stars with $T_{\text{eff}} \geq 16\,000\text{ K}$, whereas the homogeneous winds exist only for silicon rich stars with $T_{\text{eff}} = 14\,000\text{ K}$. From this we conclude that main-sequence stars with $T_{\text{eff}} \lesssim 15\,000\text{ K}$ that do not have enhanced silicon abundance do not have any homogeneous winds (i.e., winds composed of hydrogen, helium, and heavier elements).

We failed to find a wind solution for T16 model with overabundant iron $[Fe/H] = 2$. The test using the wind condition Eq. (3) showed, that the radiative force is unable to drive wind close to the star in slightly supersonic region as a result of strong

flux redistribution. We also suppose that there is not a homogeneous wind in this case.

Abbott (1979) distinguishes two wind limits in H-R diagram. In stars above the static limit the wind can be self-initiated, i.e., the radiative force is so strong that a static atmosphere is not possible. All these stars should have winds. In stars below the static limit and above the wind limit the wind can be maintained if it already exists. These stars may have or may not have winds depending on initial conditions. The inspection of the results of model atmosphere calculations shows that all model stars lie below the static limit. The derived threshold at $T_{\text{eff}} \approx 15\,000\text{ K}$ corresponds to the wind limit. In main-sequence stars our detected wind limit is by roughly 2000 K higher than that derived by Abbott (1979), most likely as a result of more realistic model atmosphere fluxes. Stars below the wind limit may still have a pure metallic wind (Babel 1995).

5. Observational consequences

5.1. Comparison of UV line profiles

The comparison of observed and predicted wind line profiles would be the most natural test of the derived mass-loss rates. However, this could be complicated in the domain of main-sequence B stars studied here. Note that except the clumping problem present in more luminous hot stars (e.g., Sundqvist et al. 2011, Šurlan et al. 2012) also the weak wind problem may complicate the situation in main-sequence B stars. Consequently, here we discuss also indirect mass-loss rate indicators and postpone a detailed study of wind line profiles for a subsequent study.

We note that some studies concentrate on a detailed description of the line profiles, that might be contributed to the winds, rather than on the wind parameter determination. In some cases this could be a safer option, because resonance lines may originate both in the wind and in the atmosphere. Detailed atmosphere models are necessary to judge whether the line originates in the wind or in the atmosphere (Hubený et al. 1986). Slettebak (1994) concludes that Si IV absorption line profiles are present up to a spectral type of B8 ($T_{\text{eff}} = 11\,600\text{ K}$), while he founds that Si IV edge velocities and equivalent widths do not vary significantly with the spectral type for stars later than about B5 ($T_{\text{eff}} = 15\,500\text{ K}$, see Figs. 4, 10 therein). This is in a rough agreement with our detected wind limit at $T_{\text{eff}} \approx 15\,000\text{ K}$. The C IV lines are visible up to a spectral type of B3 ($T_{\text{eff}} = 19\,100$) in standard (i.e., non-Be) stars in agreement with their negligible contribution to the radiative force in these stars (see Table 4). The observed variations of Si IV (or C IV) resonance line profiles may be tentatively explained if in the stars of the earlier spectral type than B5 (or B3 in the case of C IV lines) we observe absorption due to the wind, while in the later ones the absorption in Si IV lines originates in the atmosphere.

5.2. Mass-loss rates of magnetic B stars

Oskinova et al. (2011) derived the mass-loss rate for magnetic B type stars from the ultraviolet line profiles taking into account the X-ray emission. This could be crucial in B star domain (similar to late O dwarfs, Martins et al. 2005) thanks to a strong influence of X-rays on the wind ionization equilibrium. Oskinova et al. (2011) provide two mass-loss rate estimates derived from C IV and Si IV lines. These estimates differ by up to 1 dex, probably as a result of uncertain wind ionization state.

Table 5. Comparison of mass-loss rates derived by Oskinova et al. (2011) from Si IV lines and the ones predicted from the stellar effective temperature using Eq. (1).

Star	T_{eff} [K]	$\log(\dot{M}/1\,M_{\odot}\text{ year}^{-1})$	
		Oskinova et al.	prediction Eq. (1)
τ Sco	30 700	-8.6	-8.6
β Cep	25 100	-9.1	-9.2
ξ^1 CMa	27 000	-10	-8.9
V2052 Oph	23 000	-9.7	-9.6
ζ Cas	20 900	-9.7	-10.2

Here we selected the mass-loss rates derived from Si IV lines, as these lines always give higher mass-loss rate. The weaker C IV lines can be explained by, e.g., a lower ionization fraction of C IV than derived in the models. We note that the opposite (lower mass-loss rate with stronger Si IV lines) would be more difficult to explain. In Table 5 we compare these mass-loss rates derived from observations with predicted ones derived using Eq. (1) for effective temperature given in Oskinova et al. (2011, see also Table 5) for studied magnetic stars. The mass-loss rates derived from observations and the predicted ones differ in most cases by no more than 0.1 dex, consequently we conclude that there is a satisfactory agreement between observation and theory in this case.

The H α emission coming from the material trapped in the corotating magnetosphere is typically observable for the stars with effective temperature higher than about 16 000 K (Zboril et al. 1997, Petit et al. 2013). The magnetosphere is filled by the stellar wind, consequently this anticipated effective temperature limit for stars with magnetospheric H α emission may be explained by the disappearance of homogeneous wind at $T_{\text{eff}} \approx 15\,000\text{ K}$.

5.3. Rotational braking of Bp stars

The helium rich star σ Ori E shows rotational braking (Townsend et al. 2010) that can be explained as the result of angular momentum loss by a magnetized wind. The spin-down time depends on the stellar parameters, polar magnetic field strength B_p , and on the wind parameters, $\tau_{\text{spin}} \sim M(v_{\infty}/\dot{M})^{1/2}/(B_p R_*)$ (ud-Doula et al. 2009).

For the stellar parameters after Hunger et al. (1989, $T_{\text{eff}} = 22\,500\text{ K}$, $M = 8.9\,M_{\odot}$, $R_* = 5.3\,R_{\odot}$) we derive from Eq. (1) corrected for the assumed radius via $\dot{M} \sim L^2 \sim R^4$ (Krtićka & Kubát 2012) the mass-loss rate $\dot{M} = 5.5 \times 10^{-10}\,M_{\odot}\text{ year}^{-1}$. This is significantly lower value than that derived by Krtićka et al. (2006) as a result of the use of model atmospheres with metal opacity and CMF line force in the wind models.

With the polar field strength $B_p = 9.6\text{ kG}$, moment of inertia constant $k = 0.05$ (Meynet & Maeder 2006) and the terminal velocity $v_{\infty} = 1690\text{ km s}^{-1}$ (see Table 2) we derive from Eq. (25) of ud-Doula et al. (2009) the spin-down time 1.7 Myr. This agrees well with the value 1.34 Myr derived from photometry (Townsend et al. 2010).

The rotation braking as the result of angular momentum loss via the magnetized wind is effective in stars with wind and magnetic field. In Fig. 5 we plot the dependence of the spin-down time (ud-Doula et al. 2009) for the solar abundance models studied here for three different values of the polar strength of the dipolar field. The spin-down time is nearly constant for stars hotter than about $T_{\text{eff}} = 23\,000\text{ K}$. At this temperature range

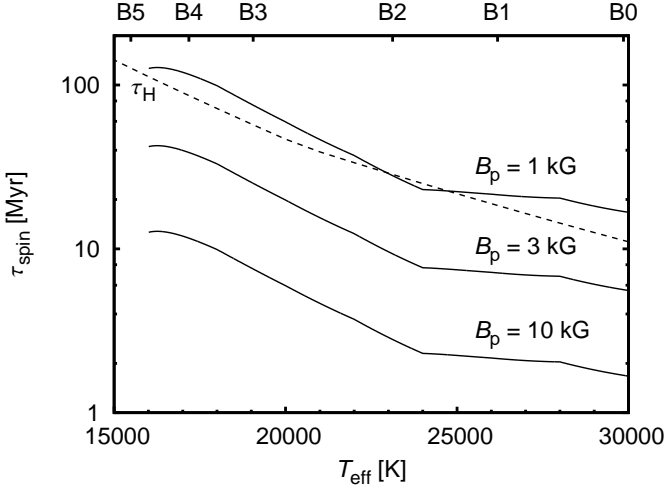


Fig. 5. The spin-down time as a result of angular momentum loss via magnetized stellar wind as a function of effective temperature for different polar field strengths. Overplotted is the main-sequence lifetime τ_H derived from the non-rotating models of Ekström et al. (2012).

the decrease of the mass-loss rate with decreasing temperature is compensated by the decrease of M/R_* ratio and v_∞ . At lower effective temperatures the spin-down time significantly increases with decreasing temperature as a result of the decrease of the mass-loss rate.

With long-term series of observations of individual stars the rotation braking with the spin-down time up to roughly 10 Myr can be detected (Mikulášek et al. 2011). From Fig. 5 this means that the rotational braking is detectable in stars with effective temperature $T_{\text{eff}} \gtrsim 22\,000$ K and medium strong field, while in cooler stars only very strong magnetic field causes detectable period changes. For stars with polar field intensity stronger than about 2 kG the spin-down time is shorter than the main-sequence life-time (see Fig. 5). Consequently, the population of stars with strong magnetic field should on average show slower rotation than stars with weaker field.

These results can be compared with the wind braking in non-magnetic stars. The time derivative of the stellar angular momentum in the case of rotational braking of uniformly rotating star can be expressed as $\dot{J} = \eta M R^2 \dot{\Omega}$, where η is a dimensionless constant given by the mass distribution in the star, and $\dot{\Omega}$ is the time derivative of the angular velocity Ω . With angular momentum loss via a nonmagnetized wind $\dot{J} = \frac{2}{3} \dot{M} R^2 \Omega$ (here $\frac{2}{3}$ comes from the integration over spherical surface) the spin-down time is $\tau_{\text{wind}} \approx \Omega / \dot{\Omega} = \frac{3}{2} \eta M / \dot{M}$. With $\eta = 0.05$ (which is appropriate for a star of a mass $M = 9 M_\odot$, Meynet & Maeder 2006) the spin-down time is by at least one order of magnitude higher than the main-sequence lifetime. Consequently, rotational braking by a nonmagnetized wind is not important in main-sequence B stars.

6. Discussion

6.1. Model simplifications

There are many effects that are neglected in the presented models. The X-ray emission strongly influences the ionization equilibrium at low effective temperatures (Martins et al. 2005).

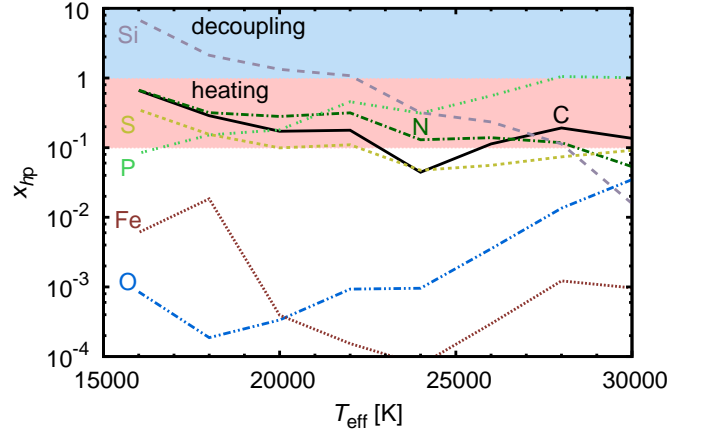


Fig. 6. The variations of the maximum relative velocity difference of individual elements and protons as a function of stellar effective temperature in the models with solar chemical composition.

However, the detailed models show that the X-ray emission does not influence the radiative force close to the star where the mass-loss rate is determined (Krtićka & Kubát 2009b). This is supported by Oskina et al. (2011) who showed, that the observed level of X-ray emission does not lead to such decrease of the radiative force and mass-loss rates that would explain problem with too weak wind line profiles in low-luminosity stars (“weak wind problem”, e.g., Bouret et al. 2003, Martins et al. 2005).

Our predicted wind mass-loss rates may be affected by a weak wind problem. However, we do not think that this is the case, because the weak wind problem may be caused by a too large cooling length in radiative shocks in the wind (Lucy & White 1980, Cohen et al. 2008, Krtićka & Kubát 2009b, Lucy 2012). However, such shocks occur well above the critical point (Owocki et al. 1988, Feldmeier et al. 1997), and consequently do not influence the mass-loss rate.

Stellar winds of hot stars have a multicomponent nature. Mostly heavier ions and free electrons are accelerated as a result of absorption of stellar radiation. The momentum acquired by these components is via Coulomb collisions transferred to hydrogen and helium. The wind can be treated as one component flow at high wind densities, while at low wind densities typical for main-sequence B star winds the effects connected with the multicomponent flow are not negligible. However, both frictional heating (Springmann & Pauldrach 1992, Krtićka & Puls 2006) or the decoupling of wind components (Owocki & Puls 2002, Votruba et al. 2007) occur typically at velocities higher than the critical one, consequently they do not affect the wind mass-loss rate, but may affect the terminal velocity.

The importance of the multicomponent effects is given by a relative velocity difference x_{hp} (Eq. (18) in Krtićka 2006) between a given element and protons. For $x_{hp} \lesssim 0.1$ the multicomponent effects are unimportant, for $x_{hp} \gtrsim 0.1$ the frictional heating typically influences the wind temperature, and for $x_{hp} \gtrsim 1$ the decoupling of components is possible. We calculated the relative velocity difference after Krtićka (2006) for all considered elements in all models. The relative velocity difference between wind components increases with radius as a result of the decrease of the wind density. In all models presented here (except T14 silicon rich models) the relative velocity difference is lower

than 1 at the critical point, consequently the decoupling does not affect the mass-loss rate which is determined at the critical point.

In some models the multicomponent effects may influence the terminal velocity. This is documented in Fig. 6, where we plot the maximum relative velocity difference x_{hp} between a given element and protons found in the wind. For the hottest stars $T_{\text{eff}} \gtrsim 28\,000$ K phosphorus may decouple from the wind. However, this likely does not significantly affect the wind, because the contribution of phosphorus to the radiative force is negligible. For stars with $T_{\text{eff}} \gtrsim 24\,000$ K the multicomponent nature of the flow leads to additional heating due to carbon, nitrogen, and silicon. For cooler stars with $T_{\text{eff}} \lesssim 22\,000$ K the decoupling of elements may occur in the outer parts of the wind. For these stars the terminal velocities in Table 2 should be corrected for multicomponent effects.

In O stars the winds are typically relatively dense and the stars themselves are luminous, consequently the typical time needed for the ionization or recombination is very short, in most cases much shorter than the typical flow-time. As a result, the advection term in NLTE equations can be safely neglected (Lamers & Morton 1976). This is no longer true in B stars (Osinkova et al. 2011) with weaker radiation field and thinner winds. We compared the ionization and recombination rates of our model ions with the inverse of the flow time v/r , where v is the radial velocity. From our models it follows that for stars with $T_{\text{eff}} \gtrsim 20\,000$ K the advection term for dominant ions is not important in the inner parts of the wind where the mass-loss rate is determined. The relative unimportance of advection term for the dominant ionization states (that drive the wind) follows from the fact, that the ionization from lower ionization state is fast, while the corresponding recombination is slow, and the opposite is true for the higher ionization state. On the other hand, in these stars the advection term may affect the population of minor ionization states and even also of dominant ones in the outer wind regions, where the lines used as observational indicators originate (Martins et al. 2005). For cooler stars than about $T_{\text{eff}} = 20\,000$ K the radiative processes become slower than the wind radial expansion, consequently the advection term may become important even for the dominant ions close to the critical point. For these stars the ionization equilibrium becomes partially frozen in the flow and advection term may affect the wind mass-loss rate.

6.2. Wind initiation

The inspection of the calculated model atmospheres shows that the radiative force in the *static* model atmospheres in main-sequence B stars does not overcome the gravity (up to $\tau_{\text{TOSS}} \approx 10^{-7}$). This means that all model stars lie below the static limit introduced by Abbott (1979). We have shown that two different solutions are possible, i.e., static atmosphere and extended atmosphere with wind. Our calculations assume that the wind was already initiated. It is not clear how the winds are initiated in this case, or even if they are initiated at all. There are several possibilities how the winds can be initiated. The radiative force on individual heavier elements overcomes the gravity in all models. This means that a metallic wind can be initiated first from the uppermost parts of the stellar atmosphere, which subsequently drives also hydrogen and helium out from the stellar atmosphere. The other possibility is that a random perturbation in the stellar atmosphere deshadows the line from the photospheric line profile leading to the initiation of an outflow. Winds may be initiated also in the pre-main sequence phase, when the star has a lower

surface gravity. The wind initiation is an interesting problem of its own which deserves a further study.

6.3. Filling the magnetosphere of σ Ori E

There are few Bp stars (including σ Ori E) that show the light variability as a result of the light absorption in the circumstellar material trapped thanks to interplay between the magnetic field and centrifugal force. The amount of the light variability enables us to estimate the mass of the magnetosphere and (with the wind mass-loss rate) the time needed to fill the clouds.

The amplitude of the σ Ori E light variability is about 0.2 mag, consequently about 20% of the stellar flux is absorbed by the clouds, implying the minimum optical depth of the clouds $\tau = 0.2$. If the magnetosphere has the same opacity as the atmosphere, then the mass of the magnetosphere can be estimated as the column mass of the atmosphere $m(\tau = 0.2)$ at the optical depth $\tau = 0.2$ multiplied by the stellar surface area. From the model atmosphere of σ Ori E we derive $m(\tau = 0.2) = 0.1 \text{ g cm}^{-2}$, giving the total mass of σ Ori E magnetosphere $M_m = 4\pi R_*^2 m(\tau = 0.2) \approx 10^{-10} M_\odot$. This should be regarded as a minimum mass, because the material could be optically thick, and consequently the optical depth can be significantly higher.

Another estimate of the mass of the magnetosphere can be derived assuming that the light scattering on free electrons dominates the opacity. In the ionized medium the opacity can not be lower than that given by the light scattering on free electrons. Then the absorbing column mass $m_e = \tau m_H / \sigma_{\text{Th}}$, where σ_{Th} is the Thomson scattering cross-section, and m_H hydrogen mass. This gives another estimate of the magnetospheric mass $M_m \approx 4\pi R_*^2 m_e = 4 \times 10^{-10} M_\odot$.

From the mass-loss rate of σ Ori E given in Sect. 5.3 we can conclude, that a minimum typical time needed to fill the magnetosphere of a star similar to σ Ori E is about one year. This is by two orders of magnitude shorter than the breakout time of the magnetosphere estimated by Townsend & Owocki (2005). From this we can conclude that many other Bp stars should show clear signatures of the matter trapped in the magnetosphere. However this is not the case, because such stars are very rare. Consequently, we can infer that there has to be some yet unknown process that incessantly removes the material deposited by the winds from the magnetospheres of the majority of Bp stars (Neiner et al. 2012).

6.4. How to couple wind and peculiarity?

Some B and A stars show chemical peculiarity caused by a radiative diffusion (see, e.g., Romanyuk 2007, for a review). The slow motion caused by the wind in the atmosphere interacts with diffusion and may modify the observed abundance anomalies. The interplay between winds and peculiarity depends on the wind mass-loss rate and the result is therefore different for stars with different effective temperatures or spectral types.

In helium rich stars a very weak wind with the mass-loss rate of the order of $10^{-13} - 10^{-12} M_\odot \text{ year}^{-1}$ is required to explain the overabundance of helium (Vauclair 1975, Vauclair et al. 1991). Typically, the helium rich stars span the temperature range of about $T_{\text{eff}} = 18\,000 - 23\,000$ K (Zboril et al. 1997, Hunger & Groote 1999). For stars in this temperature range the solar abundance mass-loss rate predictions give mass-loss rate by one to two orders of magnitude higher than that required by a diffusion theory. Such large mass-loss would destroy any chem-

ical peculiarity (Vick et al. 2011). On the other hand, helium rich regions are typically metal poor (Khokhlova et al. 2000, Bohlender et al. 2010), implying lower wind mass-loss rate. It seems that the helium overabundance may be maintained if it already exists, but it is not clear how the atmosphere could evolve to such state. Possibly, during the star formation the line-driven wind mass-loss rate increases as the effective temperature increases (Palla & Stahler 1992), leading to helium overabundance at the time of appropriate mass-loss rate. We also note that in the presence of the magnetic field the surface mass-flux \dot{m} is proportional to the tilt θ_B of the wind with respect to the local vertical direction, $\dot{m} \sim \cos^2 \theta_B$ (Owocki & ud-Doula 2004). This could be another reason for the decrease of the wind mass-loss rate to the values required by the diffusion theory in stars with overabundant helium.

In chemically peculiar stars with low effective temperatures ($T_{\text{eff}} \leq 15\,000\text{ K}$) the interplay of peculiarity and winds with mass-loss rate of the order of $10^{-14} - 10^{-12} M_{\odot} \text{ year}^{-1}$ should lead to observable overabundances of oxygen or neon (Landstreet et al. 1998). Oxygen overabundances are not observed, possibly implying the absence of such winds in these stars. This is in agreement with our finding that stars in this temperature range do not have any homogeneous line-driven wind. On the other hand, Michaud et al. (2011) argue that some mixing is required to explain the observed abundances in Sirius A, possibly with the stellar wind with mass-loss rates $10^{-13} M_{\odot} \text{ year}^{-1}$, what is not expected from our models. These stars could have pure metallic wind with mass-loss rates by about three orders of magnitude lower (Babel 1995), which is too weak to cause any substantial mixing. Possibly, the required mixing is caused by the turbulence.

Despite this qualitative agreement some open questions remain. For example, the chemically peculiar star CU Vir shows pulsed radio emission (Trigilio et al. 2000, Kellett et al. 2007), whose explanation requires a wind mass-loss rate of about $10^{-12} M_{\odot} \text{ year}^{-1}$ (Leto et al. 2006). However, stars with the effective temperature $T_{\text{eff}} = 13\,000\text{ K}$ of CU Vir (Kuschnig et al. 1999) can have purely metallic wind with the mass-loss rate by about three magnitudes lower (Babel 1995). It is not clear how to solve this disagreement. Possibly, the wind could originate from silicon-rich parts of CU Vir surface, but the predicted mass-loss rate (see Table 2) is still at least by the order of magnitude too low.

Chemically peculiar stars typically display inhomogeneous surface distribution of elements with relative elemental abundance differences reaching up to few orders of magnitude (e.g., Briquet et al. 2004, Lehmann et al. 2007, Bohlender et al. 2010). As a result of the dependence of the mass-loss rates on abundance (see Table 2) the mass flux from individual surface elements varies with location on the stellar surface. Moreover, the tilting of the flow in the presence of the magnetic field (Owocki & ud-Doula 2004) and possibly also the Zeeman effect influence the mass-loss rate. These effects may contribute to the observed rotational variability of the strength of ultraviolet resonance lines in Bp stars (Shore & Brown 1990).

6.5. Winds of fast rotating stars

The B star mass-loss rates are very sensitive to the stellar effective temperature. For fast rotating stars where the gravity darkening becomes important this leads to a large ratio of polar to equatorial mass-loss rate and density. Taking as an example the star HR 7355 rotating at about 90 % of its critical rotational velocity (Rivinius et al. 2013) with polar effective temperature

19 800 K and equatorial one 15 700 K the mass-loss rate formula Eq. (1) yields the polar to equatorial mass-loss rate ratio of about 40. Here we neglected the nonradial component of the radiative force (Owocki et al. 1996), but still this result shows that the wind asymmetries in fast rotating main-sequence B stars can be enormous.

7. Conclusions

We calculate NLTE radiatively driven wind models of main-sequence B stars with CMF line force. We provide the wind mass-loss rate predictions as a function of the stellar effective temperature. The early B stars have line driven winds with mass-loss rates of the order of $10^{-9} M_{\odot} \text{ year}^{-1}$. For the cooler stars the mass-loss rate strongly decreases with their effective temperature, so the solar-metallicity main sequence B stars with effective temperatures lower than about 15 000 K do not have any homogeneous line-driven wind. This general picture qualitatively agrees with observations of UV resonance lines and with recent B star mass-loss rate determinations.

Winds of main-sequence B stars are driven mainly by carbon, nitrogen and silicon. In the winds of stars with $T_{\text{eff}} \lesssim 22\,000\text{ K}$ the silicon driving dominates.

The mass-loss rates depend on the elemental abundances. For elements that do not significantly alter the emergent model atmosphere flux the mass-loss rate increases with increasing abundance. However, for elements that significantly influence the emergent flux (most notably iron) the mass-loss rate may decrease with increasing abundance of a given element. The dependence of the radiative force on the silicon abundance in the coolest stars studied here is so strong, that wind may be possible even below the solar-abundance wind limit at $T_{\text{eff}} = 15\,000\text{ K}$.

We discuss the implications of our models for the rotational braking, filling the magnetosphere of Bp stars and chemical peculiarity.

Acknowledgements. This work was supported by grant GA ĆR 13-10589S.

References

- Abbott, D. C. 1979, in *Mass loss and evolution of O-type stars*, IAUS 83 (Dordrecht: D. Reidel Publishing Co.), 237
- Abbott, D. C. 1980, *ApJ*, 242, 1183
- Abbott, D. C. 1982, *ApJ*, 259, 282
- Asplund M., Grevesse N., Sauval A. J., Scott P., 2009, *ARA&A*, 47, 481
- Babel, J. 1995, *A&A*, 301, 823
- Babel, J. 1996, *A&A*, 309, 867
- Bohlender, D. A., Rice, J. B., & Hechler, P. 2010, *A&A*, 520, A44
- Bouret, J.-C., Lanz, T., Hillier, D. J., Heap, S. R., Hubeny, I., Lennon, D. J., Smith, L. J., Evans, C. J. 2003, *ApJ*, 595, 1182
- Briquet, M., Aerts, C., Lüftinger, T. et al. 2004, *A&A*, 413, 273
- Castor, J. I., Abbott, D. C., & Klein, R. I. 1975, *ApJ*, 195, 157
- Cohen D. H., Kuhn M. A., Gagné M., Jensen E. L. N., Miller N. A., 2008, *MNRAS*, 386, 1855
- de Jager, C., Nieuwenhuijzen, H., & van der Hucht, K. A. 1988, *A&AS*, 72, 259
- Ekström, S., Georgy, C., Eggenberger, P. et al. 2012, *A&A*, 537, A146
- Feldmeier, A., & Shlosman, I. 2000, *ApJ*, 532, L125
- Feldmeier, A., Puls, J., Pauldrach, A. W. A., 1997, *A&A*, 322, 878
- Gayley, K. G. 1995, *ApJ*, 454, 410
- Gayley, K. G., & Owocki, S. P. 1994, *ApJ*, 434, 684
- Gvaramadze, V. V., Langer, N., & Mackey, J. 2012, *MNRAS*, 427, L50
- Harmanec, P. 1988, *Bull. Astron. Inst. Czechosl.* 39, 329
- Hubeny, I., Harmanec, P., & Štefl, S. 1986, *BAICz*, 37, 370
- Huenemoerder, D. P., Oskina, L. M.; Ignace, R. et al. 2012, *ApJL*, 756, 34
- Hummer, D. G., Berrington, K. A., Eissner, W., et al. 1993, *A&A*, 279, 298
- Hunger, K., & Groote, D. 1999, *A&A*, 351, 554
- Hunger, K., Heber, U., & Groote, D. 1989, *A&A*, 224, 57
- Kellett, B. J., Graffagnino, V., Bingham, R., Muxlow, T. W. B., & Gunn, G. A. 2007, *arXiv:astro-ph/0701214v1*

- Khokhlova, V. L., Vasilchenko, D. V., Stepanov, V. V., & Romanyuk, I. I. 2000, *AstL*, 26, 177
- Krtićka, J. 2006, *MNRAS*, 367, 1282
- Krtićka, J., & Kubát, J. 2009a, *A&A*, 493, 585
- Krtićka, J., & Kubát, J. 2009b, *MNRAS*, 394, 2065
- Krtićka J., Kubát J., 2010, *A&A*, 519, A50
- Krtićka, J., Kubát, J. 2012, *MNRAS*, 427, 84
- Krtićka, J., Kubát, J., Groote, D. 2006, *A&A*, 460, 145
- Kubát, J., Puls, J., & Pauldrach, A. W. A. 1999, *A&A*, 341, 587
- Kupka, F., Piskunov, N. E., Ryabchikova, T. A., Stempels, H. C., & Weiss, W. 1999, *A&AS* 138, 119
- Kuschnig, R., Ryabchikova, T. A., Piskunov, N. E., Weiss, W. W., & Gelbmam, M. J. 1999, *A&A*, 348, 924
- Lamers, H. J. G. L. M., Snow, T. P., & Lindholm D. M. 1995, *ApJ*, 455, 269
- Lamers, H. J. G. L. M., & Morton, D. C. 1976, *ApJS* 32, 715
- Landstreet, J. D. & Borra, E. F. 1978, *ApJL*, 224, 5
- Landstreet, J. D., Dolez, N., & Vauclair, S. 1998, *A&A*, 333, 977
- Lanz T., Hubeny I., 2003, *ApJS*, 146, 417
- Lanz T., Hubeny I., 2007, *ApJS*, 169, 83
- Lehmann, H., Tkachenko, A., Fraga, L., Tsymbal, V., & Mkrtichian, D. E. 2007, *A&A*, 471, 941
- Leto, P., Trigilio, C., Buemi, C. S., Umana, G., & Leone, F. 2006, *A&A*, 458, 831
- Lucy L. B. 2012, *A&A*, 544, A120
- Lucy L. B., & White, R. L., 1980, *ApJ*, 241, 300
- Marcolino, W. L. F., Bouret, J.-C., Martins, F., et al. 2009, *A&A*, 498, 837
- Martins, F., Schaefer, D., Hillier, D. J., et al. 2005, *A&A*, 441, 735
- Martins, F., Schaefer, D., Hillier, D. J., et al. 2005, *A&A*, 441, 735
- Mkrtichian, D. E. 2007, *A&A*, 471, 941
- Meynet, G., & Maeder, A. 2006, *Stars with the B[e] Phenomenon*, ed. M. Kraus & A. S. Miroshnichenko, ASP Conference Series, Vol. 355, 27
- Meynet, G., Ekström, S., & Maeder, A. 2006, *A&A*, 447, 623
- Michaud, G. 2004, in *The A-Star Puzzle*, IAU Symposium No. 224, eds. J. Zverko, J. Žižňovský, S. J. Adelman, & W. W. Weiss (Cambridge: Cambridge Univ. Press), 173
- Michaud, G., Richer, J., & Vick, M. 2011, *A&A*, 534, A18
- Mihalas, D., Kunasz, P. B., & Hummer, D. G. 1975, *ApJ*, 202, 465
- Mikulášek, Z., Krtićka, J., Henry, G. W. et al. 2011, *A&A*, 534, L5
- Molnar, M. R. 1973, *ApJ*, 179, 527
- Najarro, F., Hanson, M. M., & Puls, J. 2011, *A&A*, 535, A32
- Neiner, C., Landstreet, J. D., Alecian, E. et al. 2012, *A&A*, 546, A44
- Oskinova, L. M., Todt, H., Ignace, R. et al. 2011, *MNRAS*, 416, 1456
- Owocski, S. P., & Puls, J. 2002, *ApJ*, 568, 965
- Owocski, S. P., & ud-Doula, A. 2004, *ApJ*, 600, 1004
- Owocski, S. P., Castor, J. I., Rybicki, G. B. 1988, *ApJ*, 335, 914
- Owocski, S. P., Cranmer, S. R., & Gayley, K. G. 1996, *ApJL*, 472, 115
- Palla, F., & Stahler, S. W. 1992, *ApJ*, 392, 667
- Pauldrach, A. W. A., Hoffmann, T. L., & Lennon, M. 2001, *A&A*, 375, 161
- Peterson, D. M. 1970, *ApJ*, 161, 685
- Petit, V., Owocski, S. P., Wade, G. A. et al. 2013, *MNRAS*, 429, 398
- Piskunov, N. E., Kupka, F., Ryabchikova, T. A., Weiss, W. W., & Jeffery, C. S. 1995, *A&AS*, 112, 525
- Puls, J., Springmann, U., & Lennon, M. 2000, *A&AS*, 141, 23
- Puls, J., Vink, J. S., & Najarro, F. 2008, *A&ARv*, 16, 209
- Pyper, D. M., Ryabchikova, T., Malanushenko, V. et al. 1998, *A&A*, 339, 822
- Rivinius, T., Townsend, R. H. D., Kochukhov, O. et al. 2013, *MNRAS*, 429, 177
- Romanyuk, I. I. 2007, *Astrophysical Bulletin*, 62, 62
- Shore, S. N., & Brown, D. N. 1990, *ApJ*, 365, 665
- Seaton, M. J., Zeippen, C. J., Tully, J. A., et al. 1992, *Rev. Mexicana Astron. Astrofis.*, 23, 19
- Slettebak, A. 1994, *ApJS*, 94, 163
- Springmann, U. W. E., & Pauldrach, A. W. A. 1992, *A&A*, 262, 515
- Sundqvist J. O., Puls J., Feldmeier, A., Owocski S. P., 2011, *A&A*, 528, A64
- Šurlan B., Hamann W.-R., Kubát J., Oskinova L., Feldmeier A., 2012, *A&A* 541, A37
- Townsend, R. H. D., & Owocski, S. P. 2005, *MNRAS*, 357, 251
- Townsend, R. H. D. Owocski, S. P., & Groote D. 2005, *ApJ*, 630, L81
- Townsend, R. H. D., Oksala, M. E., Cohen, D. H., Owocski, S. P., & ud-Doula, A. 2010, *ApJ*, 714, 318
- Trigilio, C., Leto, P., Leone, F., Umana, G., & Buemi, C. S. 2000, *A&A*, 362, 281
- ud-Doula, A., Owocski, S. P., & Townsend, R. H. D. 2009, *MNRAS*, 392, 1022
- Unglaub, K. 2008, *A&A*, 486, 923
- Vauclair, S. 1975, *A&A*, 45, 233
- Vauclair, S., Dolez, N., & Gough, D. O. 1991, *A&A*, 252, 618
- Vick, M., Michaud, G., Richer, J., & Richard, O. 2011, *A&A*, 526, A37
- Vink, J. S., de Koter, A., & Lamers, H. J. G. L. M. 2001, *A&A*, 369, 574
- Votruba, V., Feldmeier, A., Kubát, J., & Rätz, D. 2007, *A&A*, 474, 549
- Yoon, S.-C., Langer, N., & Norman, C. 2006, *A&A*, 460, 199
- Zboril, M., North, P., Glagolevskij, Yu. V., & Betrix, F. 1997, *A&A*, 324, 949

